Journal of
Composites Science

MDPI

Article

Inductive Thermal Effect on Thermoplastic Nanocomposites with Magnetic Nanoparticles for Induced-Healing, Bonding and Debonding On-Demand Applications

Maria Kanidi, Niki Loura, Anna Frengkou, Tatjana Kosanovic Milickovic, Aikaterini-Flora Trompeta and Costas Charitidis *

Research Lab of Advanced, Composite, Nanomaterials and Nanotechnology (R-NanoLab), School of Chemical Engineering, National Technical University of Athens, 9 Heroon Polytechniou St., Zographos, GR-157 73 Athens, Greece
* Correspondence: charitidis@chemeng.ntua.gr; Tel.: +30-210-772-4046

Abstract: In this study, the heating capacity of nanocomposite materials enhanced with magnetic nanoparticles was investigated through induction heating. Thermoplastic (TP) matrices of polypropylene (PP), thermoplastic polyurethane (TPU), polyamide (PA12), and polyetherketoneketone (PEKK) were compounded with 2.5–10 wt.% iron oxide-based magnetic nanoparticles (MNPs) using a twin-screw extrusion system. Disk-shape specimens were prepared by 3D printing and injection molding. The heating capacity was examined as a function of exposure time, frequency, and power using a radio frequency (RF) generator with a solenoid inductor coil. All nanocomposite materials presented a temperature increase proportional to the MNPs' concentration as a function of the exposure time in the magnetic field. The nanocomposites with a higher concentration of MNPs presented a rapid increase in temperature, resulting in polymer matrix melting in most of the trials. The operational parameters of the RF generator, such as the input power and the frequency, significantly affect the heating capacity of the specimens, higher input power, and higher frequencies and promote the rapid increase in temperature for all assessed nanocomposites, enabling induced-healing and bonding/debonding on-demand applications.

Keywords: thermoplastic nanocomposites; hysteresis induction heating; magnetic nanoparticles; induced healing; bonding/debonding on-demand

Citation: Kanidi, M.; Loura, N.; Frengkou, A.; Milickovic, T.K.; Trompeta, A.-F.; Charitidis, C. Inductive Thermal Effect on Thermoplastic Nanocomposites with Magnetic Nanoparticles for Induced-Healing, Bonding and Debonding On-Demand Applications. *J. Compos. Sci.* **2023**, *7*, 74. https://doi.org/10.3390/jcs7020074

Academic Editor: Francesco Tornabene

Received: 29 December 2022
Revised: 22 January 2023
Accepted: 3 February 2023
Published: 9 February 2023

1. Introduction

Thermoplastic (TP) nanocomposites create high-quality and affordable materials with multifunctional properties and, thus, attract strong interest for both scientific research and applications at industrial level [1–5]. Many studies focused on the preparation and characterization of TP nanocomposites, where polymeric matrices and nanostructured fillers, such as carbon nanotubes, carbon nanofibers, and metallic or inorganic nanoparticles, are combined and present improved properties compared to the conventional composites [6–9]. The improved properties of TP nanocomposites are attributed to the high surface area of the fillers, allowing interphase interactions that result in functional materials with extraordinary properties, which are suitable for several applications such as packaging materials, sensors, thermal and electrical insulation in the construction sector, composites for automotive and health care industries, etc. [10–17]. Moreover, the inclusion of iron oxide fillers in elastomeric matrices not only improves the mechanical, actuation, and magnetic properties [16] but also tunes their mechanical performance with the presence or absence of a magnetic field [17].

Another potential application of TP nanocomposites enhanced with magnetic nanoparticles (MNPs) is their use in adhesive joining systems. Through induction heating, MNPs act as the susceptors of a high-strength electromagnetic field, convert the energy of the

field, and generate heat in nanocomposite materials by the hysteresis mechanism [18]. TP nanocomposites reinforced with metallic ferromagnetic nanoparticles, such as iron oxide (Fe_3O_4) nanoparticles, which are attractive susceptor materials for induction heating due to their strong magnetic permeability, can be used in biotechnology, medicine, and sensing applications, due to their low toxicity and biocapability [18–21]. Until now, the application of Fe_3O_4 nanoparticles in adhesive joining systems has rarely been reported, and their heating behavior has not been extensively studied. Recently, added ferrimagnetic nanoparticles to a poly(ethylene-methacrylic acid) thermoplastic adhesive enabled rapid self-heating without negatively affecting the lap shear strength [22]. Through induction heating technology, TP matrices with MNPs are heated to a molten state, and then the melted polymer chains can interdiffuse and generate a strong joint. In many cases, pressure at the damaged point should be applied to achieve an efficient bonding.

Another application where induction heating technology can be exploited in TPs is the debonding on-demand approach. In repair or recycling applications, it is often necessary to separate materials, often of a dissimilar nature (for example, composites and aluminum). This is usually accomplished via the application of large mechanical forces and extremely high temperatures, both of which can damage parts and preclude their recovery. Thus, there is a need for easily dismantlable adhesive joints that can be separated with an external stimulus (debonding on-demand). The capability to achieve local debonding is advantageous when considering the maintenance repair and operations (MRO) of multi-functional composite components. For example, it may be possible to detach and remove localized features, in order to implement smaller scale repairs. Additionally, the same capability may be deployed as part of the end of life (EoL) disassembly procedure for recycling the individual parts. The disassembly process through induction heating technology is very promising for the development of debonding on-demand applications, supporting the MRO in the aerospace, automotive, and other industries, in the frame of new repair and restoration techniques. The idea is to introduce a thin layer of thermoplastic iron oxide nanocomposite through additive manufacturing technologies, between two composite parts, to make the disassembly easier, not only for conventional composite parts but also for composite parts with new multifunctional architectures (e.g., those that have been manufactured by additive manufacturing technologies or advanced composite manufacturing technologies, such as automatic tape laying (ATL)). By applying an electromagnetic field to TP composites with MNPs, local melting occurs due to the distribution of the generated heat in the polymer matrix, allowing facile debonding from the substrates. Induction heating technology provides a high heating efficiency, to heat preferentially joint materials and bond and/or debond on-demand complex systems [21–25].

Finally, induction heating can be used for the induced self-healing of TP nanocomposites with MNPs. Most self-healing composites with MNPs are designed to recover the mechanical, magnetic, and other functional properties. Particle types as well as their size, distribution, shape, and dispersion in the polymer matrix are crucial parameters for controlling the magnetic properties of the composites and tuning the inductive heating and healing capabilities [26]. Recently, Oberhausen and Kickelbick [27] developed nanocomposites based on anionic methacrylate-based copolymers and surface-functionalized cationic iron oxide particles, which showed promising self-healing. The superparamagnetic iron oxide nanoparticles introduced magnetic properties and induced heat with an external alternating magnetic field, resolving healing at the lower macroscopic temperatures necessary for conventional healing.

In this work, TP matrices of polypropylene (PP), thermoplastic polyurethane (TPU), polyamide (PA12), and polyetherketoneketone (PEKK) were compounded with Fe_3O_4 MNPs through an extrusion process, producing nanocomposites in filament or pellet form. Nanocomposite samples with different MNP concentrations were prepared through additive manufacturing or injection molding, and functionality testing took place in an induction heating system to study their heating capacity. Moreover, the effect of the electromagnetic field parameters, such as frequency and power, was investigated, optimizing the

induction heating process window for the current working system for the heating capacity of the TP nanocomposites. Through induction heating technology, the bonding/debonding mechanism and induced-healing behavior of the TP nanocomposites were investigated, demonstrating functional materials for promising applications of induction-based composites' repair and adhesive joining systems with reversible joining procedures that provide easy-to-disassemble operations.

2. Materials and Methods

2.1. Extrusion Process

Compounding and filament production were conducted on a co-rotating parallel twin-screw extruder (Thermo Fisher Scientific, Karlsruhe, Germany) equipped with a gravimetric feeding system for nanoparticles. The whole system consisted of a cooling system (water- or air based, depending on the TP), a triaxial laser system for real-time inspection of the filament diameter and ovality, and a winding system. To produce the TP nanocomposites, TPU, PP, PA12, and PEKK polymers were compounded with Fe_3O_4 MNPs (PVP coated, 20 nm size, Nanografi). During the extrusion process, polymer pellets were fed into the extruder barrel, creating a melted material flow. Before the last mixing zone, MNPs were induced in the barrel and compounded with the melted TP matrix. The MNPs, in powder form, were introduced in excess in the gravimetric feeder. The rotation speed of the gravimetric feeder screw was set, to have a stable flow of particles throughout the process, taking into account the mass flow of the polymer pellets, from the volumetric feeder (mass of pellets was measured at a specific feeder speed, as presented in Table 1, for each case), for a defined time duration. The molten compounded material was then driven to the discharge end of the barrel and was extruded through a die head, forming a material strand. Then, the filament was cooled in water bath or in air (for the PEKK) and spooled at a constant stretching rate by the winding system. Initially, masterbatches of 10 wt.% content in MNPs were prepared for each polymer, which were then diluted in lower concentrations of 2.5, 5, and 7.5 wt.%. Fe_3O_4 MNPs. Pure matrix filaments and relevant specimens were also prepared as reference materials. In Table 1, the optimized process parameters (screw rotation speed, feeder rotation speed, and temperature range) that were used to produce filaments with acceptable filament diameter (1.75 ± 0.05 mm) are presented.

Table 1. Temperature profiles during extrusion process.

Temperature Zones (°C)	1	2	3	4	5	6	7	Screw Speed (rpm)	Feeder Speed (rpm)
PP	200	200	200	200	190	180	120	400	42
PA12	225	225	225	200	200	180	100	400	50
TPU	210	210	210	210	200	180	105	350	30
PEKK	323	323	310	310	305	305	290	200	8

2.2. Specimens' Preparation

For the preparation of specimens with disk-shape geometry, a 3D printer (Prusa MK3S, Figure 1) for PP and PA12 and an injection molding desktop system (Xplore micro–Injection Moulder IM12) for TPU and PEKK were employed.

For the 3D printing of the specimens, a 0.4 mm diameter stainless steel nozzle for 1.75 mm diameter filaments was used. The 3D designs were prepared using the Fusion3D program, and the printing settings and control were performed using the PrusaSlicer program. Disk-shape specimens of 25 mm diameter and 5 mm thickness were prepared for PP and PA12, with the operational conditions described in Table 2.

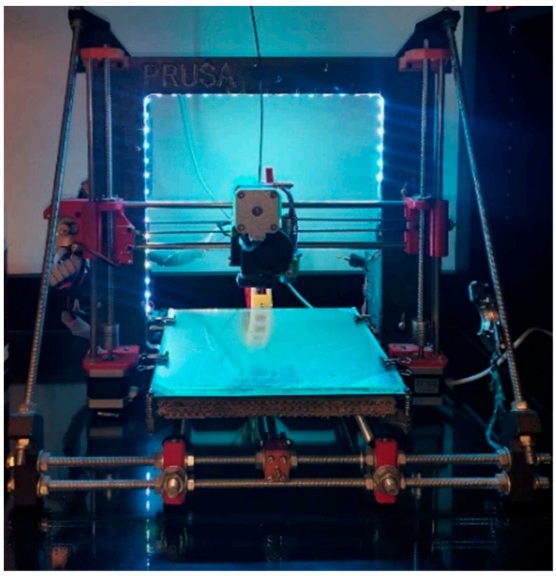

Figure 1. Prusa 3D printer used for the preparation of samples.

Table 2. The 3D printing operational conditions.

3D Printing Conditions	Nanocomposites PA12 with MNPs	Nanocomposites PP with MNPs
Temperature bed (°C)	95	80
Extruder temperature (°C)	265	235
Printing speed (mm/s)	45	25–35
Layer thickness (mm)	0.2	0.2
Fill density (%)	100	100

For TPU and PEKK, melted extruded material from the twin-screw extruder was fed directly into the hot barrel of the injection molding machine. The temperature of the chamber was the same as the extrusion temperature of the last zone for each material, while the mold temperature was 150 °C lower than the barrel temperature. The mold consisted of two circular cavities with dimensions of 25 mm × 2 mm. For PEKK specimens, the chamber temperature was 323 °C, the mold temperature was 153 °C, and the injection pressure was set at 9–11 bar.

2.3. Nanocomposite Microstructure, Morphology, and Filler Dispersion

The morphology and the elemental mapping analysis of the samples were determined by SEM using a Hitachi TM3030Plus microscope equipped with a QUANTAX 70 energy dispersive X-ray spectroscopy (EDS) analysis system. The internal structural information of composites was observed and collected by the compact desktop Bruker Micro Computational Tomography (micro-CT) 3D X-ray scan system, SkyScan 1272. The system consists of a micro-focus sealed X-ray source that operates at 20–100 kV and 10 W (<5 µm spot size at 4 W), an X-ray detector with a maximum resolution of 11Mp (4032 × 2688 pixels), and a 14bit cooled CCD fiber optically coupled to a scintillator.

2.4. Degradation and Stability of Nanocomposites

Thermogravimetric analysis was carried out with a NETZSCH/ STA 449 F5 Jupiter thermal analysis system. The instrument is accompanied with a desktop computer for the analysis of the data using the related software. The system consists of a silicon carbide furnace with a range from 25 °C to 1550 °C, a SiC heating element, and an Al_2O_3 protective tube for gas flow with a stop valve. The high-quality SiC heating element of the furnace allows a maximum operation temperature of 1550 °C. The present thermal analysis was

conducted from 50 °C to 800 °C by applying a heating step of 10 °C/min in inert N_2 atmosphere (nitrogen flow: 50 mL/min), to receive information about degradation and stability of the received polymers. Specifically, PA12 and PP were tested for their thermal stability, since they were the two nanocomposites that were 3D-printed for specimens' preparation.

2.5. Induction-Heating Testing

For the functionality testing of the TP nanocomposites, a lab-scale testing setup consisting of an RF generator TruHeat HF 5010 (Trumpf Hüttinger, Freiburg, Germany), connected to an external circuit with maximum current of 35 A, was used. The external circuit was composed of a transformer and capacitors, which formed a series resonant circuit in conjunction with an inductor (copper solenoid coil with a length of 8 cm and inner diameter of 4 cm) connected to the output. Excitation with an alternating voltage causes a periodic oscillation of current and voltage in the series circuit. The maximum permissible RF current depends on the respective operating frequency. Depending on the susceptors used, the field generated by the induction coil affects the heating patterns of the susceptors, and the field is a function of the coil geometry. In the induction heating set-up, the maximum power generated by the equipment was the maximum magnetic field power, which was 4–6 kW, working with capacitors that produce fields with frequencies of 575, 446, and 325 kHz. Nanocomposite samples were placed in the center of the solenoid coil and exposed to an electromagnetic field at pre-set parameters (Figure 2). During the exposure, distribution of heat at the sample surface was measured by an infrared (IR) thermal camera imaging system (FLIR E5). The distance between the sample and the camera was 0.3 m. The imaging system software was used to record the images and temperature vs. time. An IR camera system is a real time non-contacting measurement system of two-dimensional surface measurements. The maximum temperature values obtained in the center of the sample were recorded in 15 s time intervals to reproduce temperature–time/heating capacity curves.

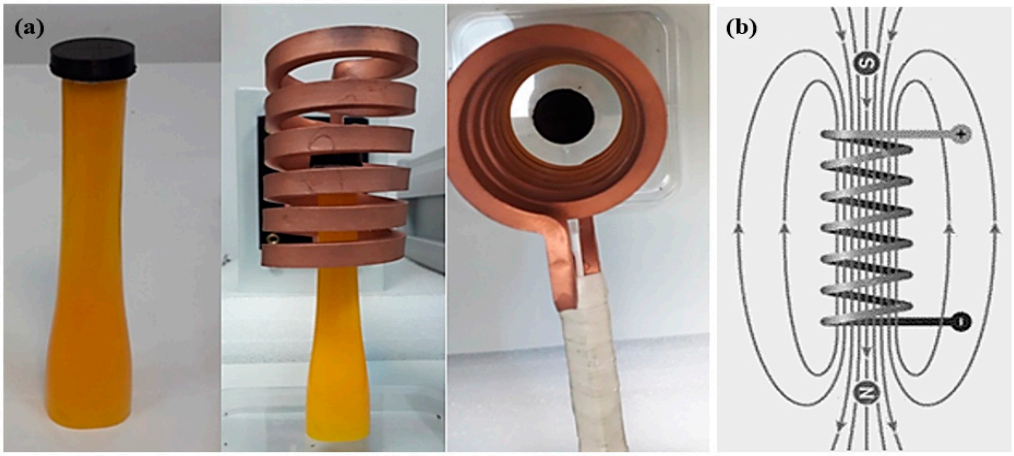

Figure 2. (**a**) Sample holder and solenoid coil for induction-heating testing and (**b**) electromagnetic field produced in solenoid coil (right).

3. Results

3.1. Manufactured Nanocomposites

The nanocomposite specimens of each composition, prepared either through 3D printing or by injection molding, were subjected to induction-heating testing. In Figure 3a, the 3D-printed specimens of PP nanocomposites are presented, while, in Figure 2b, the injection-molded specimens of PEKK are depicted, before the induction-heating testing. Moreover, a summary of all nanocomposite specimens that were prepared for testing are presented in the table included in Figure 2c.

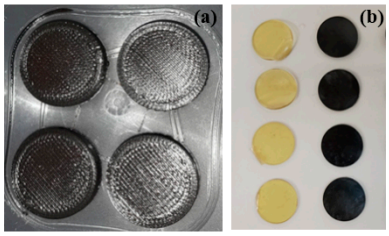

Polymer matrix	Concentration % wt. MNPs	Type of sample (c)
PP	0, 2.5, 5, 7.5, 10	3D printed
PA12	0, 2.5, 5, 7.5, 10	3D printed
TPU	0, 2.5, 5, 7.5, 10	injection molded
PEKK	0, 2.5, 5, 7.5, 10	injection molded

Figure 3. (**a**) The 3D-printed specimens of PP nanocomposites, (**b**) injection-molded specimens of pure PEKK and PEKK nanocomposites, and (**c**) specifications of samples for induction-heating testing.

3.2. Dispersion Assessment

In order to evaluate the magnetite filler distribution in the polymer matrix, elemental mapping by EDS was carried out. The mapping images and respective SEM micrographs of PA12 nanocomposites for loading of 2.5, 5, and 10 wt.% of MNPs are presented in Figure 4. The filler particles were dispersed uniformly in the nanocomposite (elemental Fe is mapped by blue-cyan color). However, some aggregate formation was observed in the mapping as well as in the SEM images, where the darker areas correspond to polymer matrices and the bright regions are iron oxide particles. With the increase in MNPs' concentration, magnetite particles are more populated, showing the formation of percolative networks.

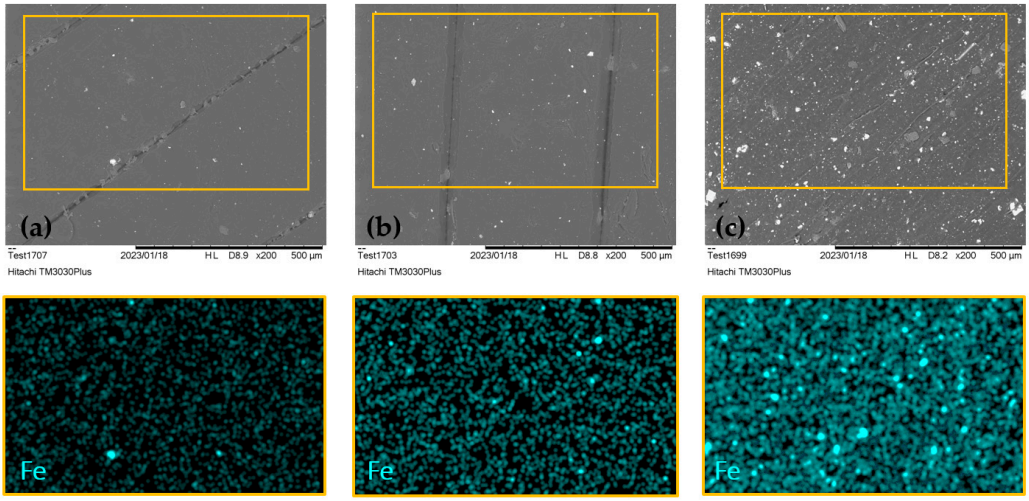

Figure 4. SEM micrographs of the surface of 3D-printed PA12/Fe_3O_4 nanocomposite samples and Fe filler distributions, as determined by elemental mapping (EDS): (**a**) 2.5 wt.%, (**b**) 5 wt.%, (**c**) 10 wt.% Fe_3O_4.

Moreover, before the induction-heating testing, a selected nanocomposite specimen of PEKK/Fe_3O_4 (10 wt.% MNPs) was subjected to micro-CT analysis. Using micro-CT analysis, features of the microscale can be observed as the resolution is approx. 10 µm, while features in the nanoscale cannot be distinguished. The particles are homogeneously dispersed in the polymeric matrix. The microscale features that are observed in Figure 5 correspond to the agglomerates of MNPs.

3.3. Thermal Stability Assessment

The present thermal stability investigation focused on PP and PA12 containing MNPs at various contents. The observed thermal behavior was connected to the dispersion of the MNPs in the polymer matrix as well as to the thermal transitions of the MNPs, which are expected to remain intact in terms of their chemical composition at high temperatures up to 800 °C. Starting with the thermal behavior of the matrix polymers, both PP and PA12 seem to be decomposed due to pyrolysis reactions in this temperature range. Even though the

onset temperature of the decomposition seems to be the same, a higher mass percentage is retained in the case of masterbatches (10 wt.%), and the residual mass is very close to the nominal weight percentage of the reinforcement, if the matrix contribution is taken into account (Figure 6). The PP onset temperature of the decomposition demonstrated an increasing trend of dependence on the content of the MNPs. The residual mass followed an increasing trend with the MNPs' content, which was slightly smaller compared to the original weight ratio (the residual mass equal was to 1.1 wt.%, 3.9 wt.%, 6.1 wt.%, and 9.4 wt.% for the 2.5 wt.%, 5 wt.%, 7.5 wt.%, and 10wt.%. PP nanocomposites, respectively). Finally, in the case of PA12, it seems that the presence of the MNPs did not at all affect the thermal decomposition behavior of the nanocomposites, while the residual mass was equal to 1.2 wt.%, 2.2 wt.%, 7.1 wt.%, and 8.5 wt.% for the 2.5 wt.%, 5 wt.%, 7.5 wt.%, and 10 wt.% PA12 nanocomposites, respectively.

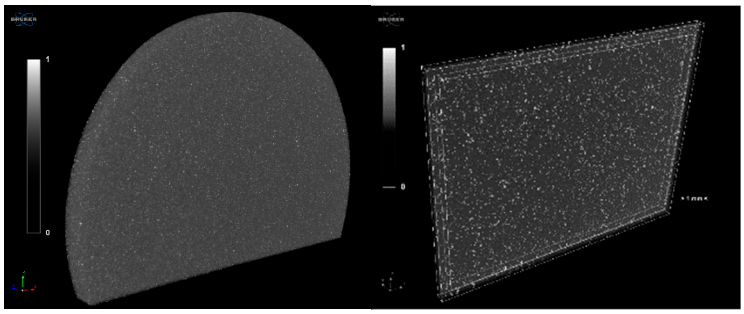

Figure 5. CTVox images of the scanned PEKK nanocomposite with 7.5/10 wt.% Fe_3O_4 (gray = PEKK matrix, and white = MNPs).

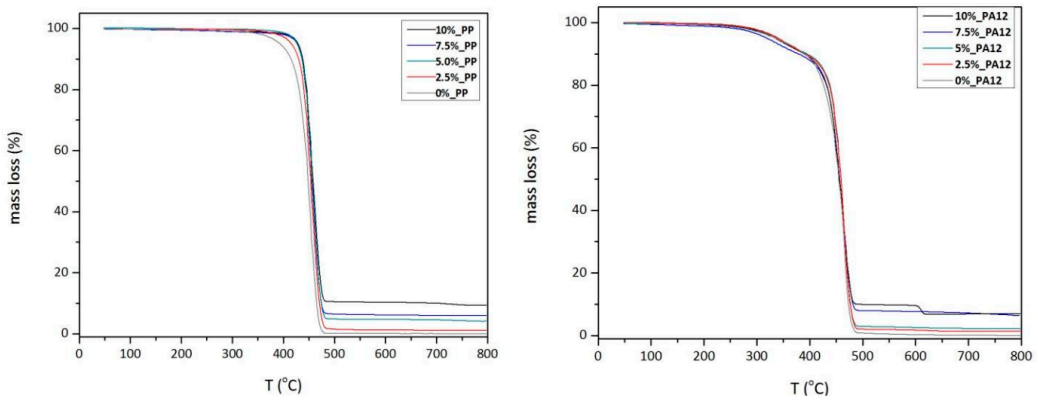

Figure 6. Thermographs of PP (**left**) and PA12 (**right**), without and with 2.5, 5, 7.5, and 10 wt.% Fe_3O_4.

3.4. Induction-Heating Testing–Heating-Capacity Evaluation

To investigate the effect of the induction heating system's operating parameters on the heating capacity of the TP nanocomposites, an extensive study varying the frequency and input power was conducted on the PP nanocomposites. The heating capacity of the samples exposed to RF fields at 575, 436, and 325 kHz frequencies, at the maximum achieved power for each frequency, is presented in Figure 7a, as a function of the exposure time. For a frequency of 575 kHz, the maximum achieved power of the RF field was 6 kW, while for a frequency of 325 kHz, it was 4 kW. Exposing PP samples to the RF field, a temperature increase was observed, which was proportional to the content of the MNPs. By increasing the mass ratio of the MNPs in the nanocomposites, a higher increase in temperature was observed [28–30]. A higher heating capacity was observed for the samples exposed to the RF field with a higher frequency, when compared to the behavior of the PP samples with the same MNPs' concentration that were exposed to fields of different frequencies. Specifically, the samples exposed to the RF field with a 575 kHz frequency reached the

melting temperature (T_m) of PP faster, compared to the samples exposed to the RF field with frequencies of 436 and 325 kHz. The PP samples exposed to a lower frequency RF field required a longer exposure time to increase their temperature and reach T_m. An RF field with a high frequency is more suitable for the inductive particle heating of compounds than RF fields with lower frequencies [28,30].

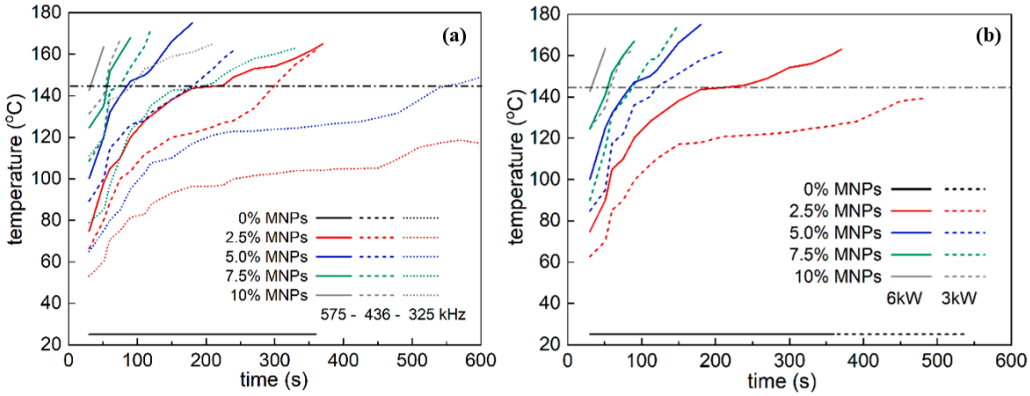

Figure 7. Increase in temperature for PP with MNPs as a function of exposure time in RF field of (**a**) 575, 436, and 325 kHz frequency; (**b**) 575 kHz and power 3 kW and 6 kW.

Another significant parameter of the RF field is its power [31]. In Figure 7b, the heating capacity as a function of the power is presented, for the PP samples exposed in the RF field with the maximum frequency (575 kHz). Samples exposed in the RF field of 3 kW power reached lower temperatures for the same exposure time compared to those exposed in the RF field of 6 kW power.

From the investigation of the induction heating system's operating parameters, it was concluded that the heating capacity is proportional to the RF frequency and power input applied; thus, the samples of PA12, TPU, and PEKK with 0, 2.5, 5, 7.5, and 10 wt.% MNPs were tested in the optimum operating conditions of the RF generator (575 kHz and 6 kW). All the samples that were examined are presented in Figure 8, which depicts the temperature increase as a function of exposure time. In the case of PP, PA12, and TPU, most of the TPs' nanocomposites reached the T_m in less than 10 min of exposure to the RF field. Samples with a lower MNPs' concentration needed a longer exposure time to present an efficient increase in temperature compared to the samples with a higher MNPs' content. In the case of PEKK, only the sample with the highest MNPs' content (10 wt.%) reached the T_m, even though significantly higher temperatures were observed compared to those of the other TP matrices. For all the TP matrices reinforced with MNPs, it is verified that heating capacity is proportional to the MNPs' concentration [28–30].

3.5. Induced Healing Evaluation

The ability to increase the temperature of a TP above the T_m is a crucial factor in order to achieve healing, since the melted polymer chains interdiffuse, reshaping cracks and making the external surface smoother. The degree of healing of the tested samples after the inductive thermal effect appeared satisfactory, since the TP surfaces became smooth, although these findings were based on visual observations (Figure 9) [32]. In the case of the PP, PA12, and TPU nanocomposites, the samples melted in a temperature range between 160 °C and 180 °C, while the PEKK nanocomposites melted at a significantly higher temperatures, close to 305 °C. Even though only the sample with the highest concentration of MNPs (10 wt.%) reached the PEKK T_m, shape deformation was observed for all the PEKK nanocomposites, as shown in Figure 9c. This can be explained by considering that the glass temperature (T_g) of PEKK is 160 °C, and, above this temperature, the polymer chains gain mobility, enabling the reshaping and cracks healing. Even though the polymer did not reach a molten state, a debonding mechanism could be possibly applied in such conditions.

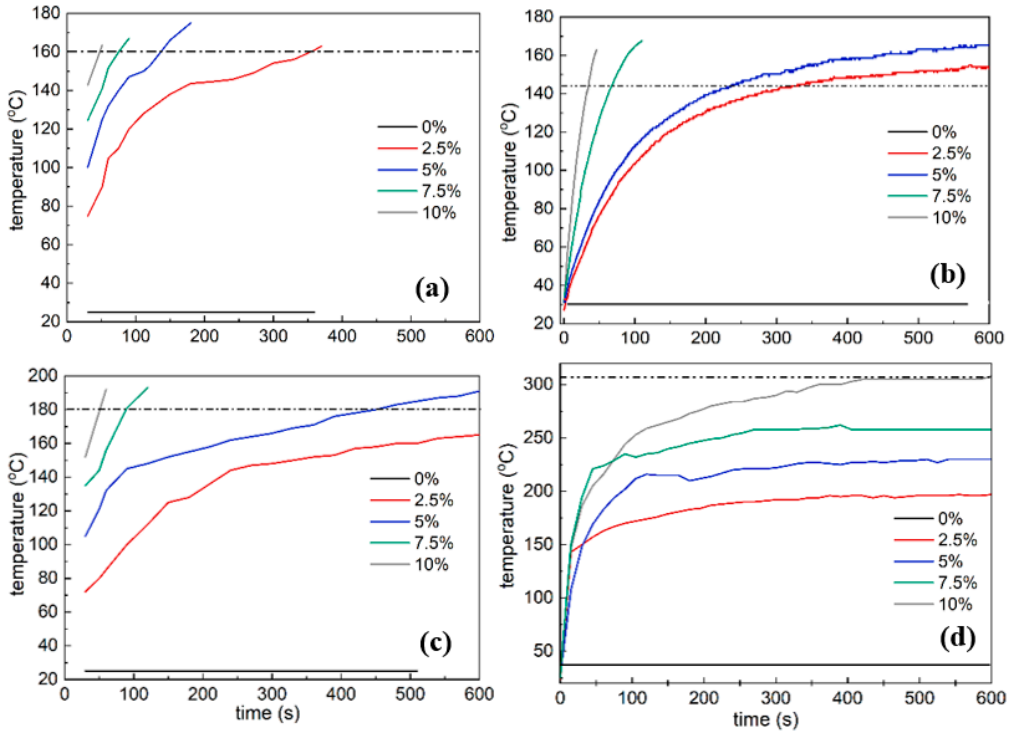

Figure 8. Heating capacity (temperature rise) of MNPs' nanocomposites: (**a**) PP, (**b**) PA12, (**c**) TPU, and (**d**) PEKK, as a function of exposure time in RF field of 575 kHz and 6 kW. Dashed lines indicate the T_m of each matrix.

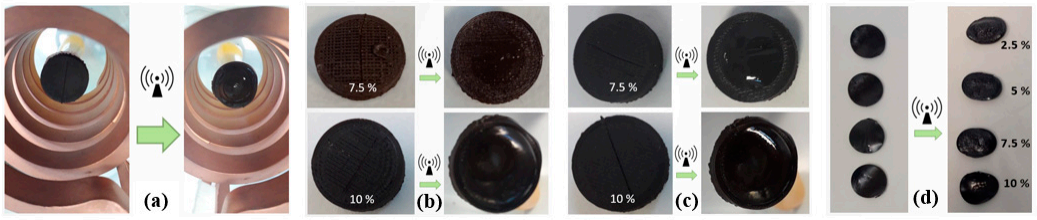

Figure 9. (**a**) Sample in the coil; nanocomposites before and after induction heating: (**b**) PP, (**c**) PA12, and (**d**) PEKK.

3.6. Bonding/Debonding On-Demand Evaluation

The concept of a bonding and debonding mechanism was investigated in "sandwich" structures with PP and PA12 nanocomposites. The schematic concept and images of the two 3D printed components of pure PP, including a part of PP with MNPs, are presented in Figure 10a. Bonding of the two PP components in one part was achieved after 1 min of exposure to RF field, simply by manually applying pressure. Additionally, debonding was demonstrated in a PA12 "sandwich" rectangular structure, which consisted of two pure PA12 components connected with a PA12 part with MNPs (Figure 10b). Exposing the PA12 "sandwich" structure to the RF field at the optimum operating conditions for less than 3 min, the nanocomposite PA12 part with the MNPs melted, and the two components of the pure PA12 were debonded, by manually applying force. Several studies reported the potential use of induction heating for the bonding/debonding of TP composite structures compared to the traditional joining methods, even though this technology has not significantly shifted to industrial applications [33,34].

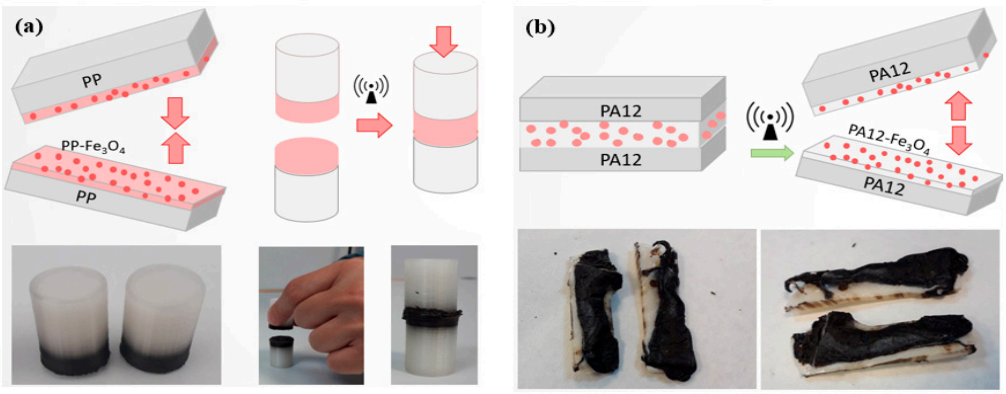

Figure 10. Schematic concept and images of (**a**) PP components with MNPs bonded by manually applying pressure, and (**b**) PA12 components with MNPs debonded by manually applying force.

4. Conclusions

Functional TP nanocomposites based on iron oxide MNPs can be triggered by an RF field and present an inductive thermal effect. All the TP nanocomposites presented a temperature increase proportional to the MNPs' concentration when exposed to the RF field. The operating parameters of the RF generator, namely, the frequency and input power, significantly affected the heating capacity of the TP nanocomposites, proportionally increasing with a higher RF frequency and generator input power. Induced healing behavior was observed for most of the TP nanocomposites that reached a temperature close to the T_m of the matrix after a short period of exposure to the RF field. The MNPs acted as susceptors, by distributing the generated heat to the polymer matrix that caused local melting and polymer chains' interdiffusion, which allowed facile bonding/debonding.

Most of the thermoplastic matrices functionalized with MNPs presented healing behavior in less than 10 min of exposure in the RF field. However, concentrations of 7.5 and 10 wt.% in MNPs allowed the thermoplastic matrices to be healed after a short exposure time in the RF field. Moreover, by applying the optimum operating conditions of the RF generator, bonding/debonding on demand was achieved between the two TP components that included a functionalized part with MNPs.

In the case of PEKK, which is a high-performance polymer and requires a high processing temperature, the nanocomposite with the highest MNPs' content (10 wt.%) reached the T_m, while those nanocomposites with a lower MNPs' content did not result in a molten state, although they presented a shape deformation. The debonding mechanism at temperatures lower than the T_m of the TP nanocomposites should be further investigated through the hysteresis heating of ferrimagnetic nanoparticles. To reach higher temperatures in the PEKK nanocomposites with a lower MNPs' concentration, several parameters that depend on the capacitors and coil geometry should be altered in the induction heating system, tailoring the input power, frequency, and distribution of the RF field.

Optimizing the process window of induction heating and addressing possible issues of this technology, the bonding/debonding concept has the potential to be further developed for scaled-up real-world applications. Induction heating technology offers an improved process efficiency with localized, constant, and precise heating; in terms of industrial applications, it can be conceivably integrated into production lines. Functional TP nanocomposites enable a faster and leaner integration into demanding structures, while the hysteresis heating of the ferrimagnetic nanoparticles in the TP matrix and bonding/debonding on demand make the repair process easier, compared to thermoset composites. Taking advantage of the hysteresis heating mechanism, TP nanocomposite materials based on MNPs constitute promising materials for the induction-based repair of composites, extending their end-of-life and being exploited in adhesive joining systems with complex geometries, enabling reversible joining procedures for sustainable solutions and providing easy-to-disassemble operations.

Author Contributions: Conceptualization, T.K.M. and A.-F.T.; methodology, M.K., N.L., A.F., T.K.M., and A.-F.T.; investigation, M.K., N.L., and A.F.; data curation, M.K.; visualization, M.K. and T.K.M.; validation, T.K.M.; writing—original draft preparation, M.K., N.L., and A.F.; writing—review and editing, T.K.M. and A.-F.T.; supervision, C.C.; project administration, C.C.; resources, C.C.; funding acquisition, C.C. All authors have read and agreed to the published version of the manuscript.

Funding: This work was funded by the Horizon 2020 Research and Innovation Actions entitled 'Recycling and Repurposing of Plastic Waste for Advanced 3D Printing Applications' (Repair3D) under GA No. 814588 and 'Digital method for improved manufacturing of next-generation multifunctional airframe parts' (DOMMINIO) under GA No. 101007022.

Data Availability Statement: Data sharing is not applicable.

Conflicts of Interest: The authors declare no conflict of interest. The funders had no role in the design of the study; in the collection, analyses, or interpretation of data; in the writing of the manuscript; or in the decision to publish the results.

References

1. Valino, A.D.; Dizon, J.R.C.; Espera, A.H., Jr.; Chen, Q.; Messman, J.; Advincula, R.C. Advances in 3D Printing of Thermoplastic Polymer Composites and Nanocomposites. *Prog. Mater. Sci.* **2019**, *98*, 101162. [CrossRef]
2. Vaithylingam, R.; Ansari, M.N.M.; Shanks, R.A. Recent Advances in Polyurethane Based Nanocomposites: A Review. *Polym. Plast. Technol. Eng.* **2017**, *56*, 1528–1541. [CrossRef]
3. Feldman, D. Polyamide nanocomposites. *J. Macromol. Sci. A* **2017**, *54*, 255–262. [CrossRef]
4. Díez-Pascual, A.M.; Naffakh, M.; Marco, C.; Ellis, G.; Gómez-Fatou, M.A. High-performance nanocomposites based on polyetherketones. *Prog. Mater. Sci* **2012**, *57*, 1106–1190. [CrossRef]
5. Peponi, L.; Puglia, D.; Torre, L.; Valentini, L.; Kenny, J.M. Processing of nanostructured polymers and advanced polymeric based nanocomposites. *Mat. Sci. Eng. R Rep.* **2014**, *85*, 1–46. [CrossRef]
6. Breuer, O.; Sundararaj, U. Big returns from small fibers: A review of polymer/carbon nanotube composites. *Polum. Compos.* **2004**, *25*, 630–645. [CrossRef]
7. Paza, H. Antimicrobial Polymers with Metal Nanoparticles. *Int. J. Mol. Sci.* **2015**, *16*, 2099–2116.
8. Steurer, P.; Wissert, R.; Thomann, R.; Mulhaupt, R. Functionalized Graphenes and Thermoplastic Nanocomposites Based upon Expanded Graphite Oxide. *Macromol. Rapid Commun.* **2009**, *30*, 316–327. [CrossRef]
9. Hiremath, A.; Murthy, A.A.; Thipperudrappa, S.; Bharath, K.N. Nanoparticles Filled Polymer Nanocomposites: A Technological Review. *Cogent Eng.* **2021**, *8*, 1991229. [CrossRef]
10. Coiai, S.; Passaglia, E.; Pucci, A.; Ruggeri, G. Nanocomposites Based on Thermoplastic Polymers and Functional Nanofiller for Sensor Applications. *Materials* **2015**, *8*, 3377–3427. [CrossRef]
11. Colijn, I.; Schroën, K. Thermoplastic bio-nanocomposites: From measurement of fundamental properties to practical application. *Adv. Colloid Interface Sci.* **2021**, *292*, 102419. [CrossRef]
12. Ismail, N.H.; Mustapha, M. A Review of Thermoplastic Elastomeric Nanocomposites for High Voltage Insulation Applications. *Polym. Eng. Sci.* **2018**, *58*, E36–E63. [CrossRef]
13. Sundarram, S.; Kim, Y.-H.; Li, W. Preparation and characterization of poly(ether imide) nanocomposites and nanocomposite foams. In *Manufacturing of Nanocomposites with Engineering Plastics*; Woodhead Publishing: Sawston, UK, 2015; pp. 61–85.
14. Golbang, A.; Mokhtari, M.; Harkin-Jones, E.; Archer, E.; Mcilhagger, A. Additive Manufacturing and Injection Moulding of High-Performance IF-WS2/PEEK Nanocomposites: A Comparative Study. *Front. Mater. Sci.* **2021**, *8*, 745088. [CrossRef]
15. Kumar, V.; Kumar, A.; Song, M.; Lee, D.-J.; Han, S.-S.; Park, S.-S. Properties of Silicone Rubber-Based Composites Reinforced with Few-Layer Graphene and Iron Oxide or Titanium Dioxide. *Polymers* **2021**, *13*, 1550. [CrossRef] [PubMed]
16. Kumar, V.; Alam, M.N.; Park, S.S. Robust magneto-rheological elastomers performance for composites based on iron oxide and carbon black in silicone rubber. *J. Polym. Res.* **2022**, *29*, 251. [CrossRef]
17. Turner, R.D.; Wingham, J.R.; Paterson, T.E.; Shepherd, J.; Majewski, C. Use of silver-based additives for the development of antibacterial functionality in Laser Sintered polyamide 12 parts. *Sci. Rep.* **2020**, *10*, 892. [CrossRef] [PubMed]
18. Mohapatra, J.; Xing, M.; Liu, J.P. Inductive Thermal Effect of Ferrite Magnetic Nanoparticles. *Materials* **2019**, *12*, 3208. [CrossRef] [PubMed]
19. Ryu, C.; Ryu, C.; Lee, H.; Kim, H.; Hwang, S.; Hadadian, Y.; Mohanty, A.; Park, I.K.; Cho, B.; Yoon, J.; et al. Highly Optimized Iron Oxide Embedded Poly(Lactic Acid) Nanocomposites for Effective Magnetic Hyperthermia and Biosecurity. *Int. J. Nanomed.* **2022**, *17*, 31–44. [CrossRef]
20. Gradinaru, L.M.; Barbalata Mandru, M.; Drobota, M.; Aflori, M.; Butnaru, M.; Spiridon, M.; Doroftei, F.; Aradoaei, M.; Ciobanu, R.C.; Vlad, S. Composite Materials Based on Iron Oxide Nanoparticles and Polyurethane for Improving the Quality of MRI. *Polymers* **2021**, *13*, 4316. [CrossRef]
21. Chen, L.; Chen, C.; Wang, P.; Song, T. Mechanisms of Cellular Effects Directly Induced by Magnetic Nanoparticles under Magnetic Fields. *J. Nanomater.* **2017**, *2017*, 1564634. [CrossRef]

22. Cheng, X.; Zhou, Y.; Charles, A.D.M.; Yu, Y.; Islam, M.S.; Peng, S.; Wang, J.; Rider, A.N.; Lim, M.; Timchenko, V.; et al. Enabling contactless rapid on-demand debonding and rebonding using hysteresis heating of ferrimagnetic nanoparticles. *Mater. Des.* **2021**, *210*, 110076. [CrossRef]
23. Zimmerer, C.; Salazar Mejia, C.; Utech, T.; Arnhold, K.; Janke, A.; Wosnitza, J. Inductive heating using a high-magnetic-field pulse to initiate chemical reactions to generate composite materials. *Polymers* **2019**, *11*, 535. [CrossRef] [PubMed]
24. Fink, B.K.; McKnight, S.H. Ferromagnetic Nano-Particulate and Conductive Mesh Susceptors for Induction-Based Repair of Composites. In Proceedings of the Army Science Conference, Norfolk, VA, USA, 15–17 June 1998.
25. Rudas, I.J. (Ed.) *Applied Mathematics and Materials*; Mathematics and Computers in Science and Engineering Series; WSEAS Press: Rome, Italy, 2015; ISBN 978-1-61804-347-4.
26. Ciardiello, R. The Mechanical Performance of Re-Bonded and Healed Adhesive Joints Activable through Induction Heating Systems. *Materials* **2021**, *14*, 6351. [CrossRef] [PubMed]
27. Oberhausen, B.; Kickelbick, G. Induction heating induced self-healing of nanocomposites based on surface-functionalized cationic iron oxide particles and polyelectrolytes. *Nanoscale Adv.* **2021**, *3*, 5589–5604. [CrossRef]
28. Suwanwatana, W.; Yarlagadda, S.; Gillespie, J.W., Jr. Influence of particle size on hysteresis heating behavior of nickel particulate polymer films. *Compos. Sci. Technol.* **2006**, *66*, 2825–2836. [CrossRef]
29. Bayerl, T.; Schledjewski, R.; Mitschang, P. Induction Heating of Thermoplastic Materials by Particulate Heating Promoters. *Polym. Polym. Compos.* **2012**, *20*, 333–342. [CrossRef]
30. Xiang, Z.; Ducharne, B.; Della Schiava, N.; Capsal, J.-F.; Cottinet, P.-J.; Coativy, G.; Lermusiaux, P.; Quyen Le, M. Induction heating-based low-frequency alternating magnetic field: High potential of ferromagnetic composites for medical applications. *Mater. Des.* **2019**, *174*, 107804. [CrossRef]
31. Muddassir, M. Development of Nano/Micro Hybrid Susceptor Sheet for Induction Heating Applications. Ph.D. Thesis, Technische Universität Kaiserslautern, Kaiserslautern, Germany, 2016.
32. Tsamasphyros, G.J.; Christopoulos, A.C. Induction heating on Thermally Remendable self-healing polymers containing magnetic nanoparticles. In Proceeding of the International Conference on Materials Science, Rome, Italy, 7–9 November 2015.
33. Ahmed, T.J.; Stavrov, D.; Bersee, H.E.N.; Beukers, A. Induction welding of thermoplastic composites—An overview. *Compos. Part A Appl. Sci. Manuf.* **2006**, *37*, 1638–1651. [CrossRef]
34. Reis, J.P.; de Moura, M.; Samborski, S. Thermoplastic Composites and Their Promising Applications in Joining and Repair Composites Structures: A Review. *Materials* **2020**, *13*, 5832. [CrossRef]